

Computational investigation on the mechanism of cobalt-catalysed alkoxy carbonylation of alkyl halides

Yanwei Cao^a, Chaoren Shen^{a,c,**}, Jie Min^b, Lin He^a, Xinxin Tian^{b,*}

^a State Key Laboratory for Oxo Synthesis and Selective Oxidation, Suzhou Research Institute of LICP, Lanzhou Institute of Chemical Physics (LICP), Chinese Academy of Sciences, Lanzhou, 730000, PR China

^b Institute of Molecular Science, Key Laboratory of Materials for Energy Conversion and Storage of Shanxi Province Shanxi University, Taiyuan, Shanxi Province, 030006, PR China

^c School of Chemistry and Molecular Engineering, East China Normal University, Shanghai, 200240, PR China

ARTICLE INFO

Keywords:

Carbonylation
Homogeneous catalyst
Cobalt carbonyl
alkyl halides
DFT

ABSTRACT

The mechanism of cobalt-catalyzed methoxycarbonylation of bromoacetonitrile and methyl 2-halogen acetate was computationally investigated by comparing three different reaction pathways with the consideration of solvation and counteraction effect. Pathway B, which goes through the addition of MeO⁻ to (RCH₂)Co(CO)₄ and the elimination of [(RCH₂)Co(CO)₃(COOMe)]⁻ to afford ester, is found to be the most kinetically favored. The previously proposed pathway A, which goes through twice S_N2 reaction, and herein proposed pathway C, which undergoes the conventional migratory CO insertion of (RCH₂)Co(CO)₄ and further methanolysis of (RCH₂CO)Co(CO)₄ intermediate, are less favored due to their higher barrier. The thermodynamic contribution of counteraction is distinct, but the mechanism preference still keeps.

Introduction

Transition metal-catalysed carbonylation is a versatile method to implant carbonyl functional group and convert bulky chemicals to value-added products with carbon monoxide [1–3]. Hydrocarbons with unsaturated carbon-carbon bond and organohalides represent two major types of electrophilic substrate for the carbonylative conversion. Owing to the presence of π-acidic CO, which would decrease the electron density on the metal centre of catalyst, the S_N2-type oxidative addition of sp³-hybridized alkyl halides through metal carbonyls is more challenging than aryl or vinyl halides [4,5]. Thus, for the carbonylation of organohalides, alkyl halides bearing electron-withdrawing group (EWG) at α position, such as α-halogen acetate and α-halogen acetonitrile, provides an important and cyanide-free alternative to achieve the carbonylative synthesis of malonate and α-nitrile carboxylate, which is hardly accessible from other carbonylation methods [6]. Since the discovery of Heck and Breslow [7], various transition metal-based homogeneous or heterogeneous catalysts have been developed for this process [8–11]. Among them, simple and inexpensive anionic cobalt carbonyl complex exhibited good catalytic activity in the relatively milder

conditions [6,12–17]. The process based on cobalt tetracarbonyl catalyst has been applied in the industrial manufacture of malonic ester [18,19]. Meanwhile, the reaction mechanism concerning the alkoxy carbonylation of alkyl halides bearing EWG received far less attention. Although there were some spectroscopic evidences about the intermediates involving the catalytic alkoxy carbonylation of alkyl halides [13,15,20,21], the proposed plausible mechanisms based on these evidences failed to support a set of clear and complete depiction about each elementary step in the reaction process. With the advancement of computational chemistry in last few decades, density function theory (DFT) [22,23] computation now can provide a useful tool to investigate each elementary step and related unstable transient intermediates in organometallic catalysis [24–27]. Herein we investigated different pathways of cobalt-catalysed alkoxy carbonylation of EWG-activated alkyl halides by using DFT computation, and hope to get a full understand of the reaction mechanism.

Regarding the cobalt-catalysed alkoxy carbonylation of alkyl halides, scheme 1 illustrated the plausible mechanism proposed in the previous reports. It was based on trans-[(RCH₂)Co(CO)₃(COOCH₃)]⁻ as one of the key reaction intermediates [13,15,20,28], which was characterized by

* Corresponding author.

** Corresponding author at: State Key Laboratory for Oxo Synthesis and Selective Oxidation, Suzhou Research Institute of LICP, Lanzhou Institute of Chemical Physics (LICP), Chinese Academy of Sciences, Lanzhou 730000, PR China.

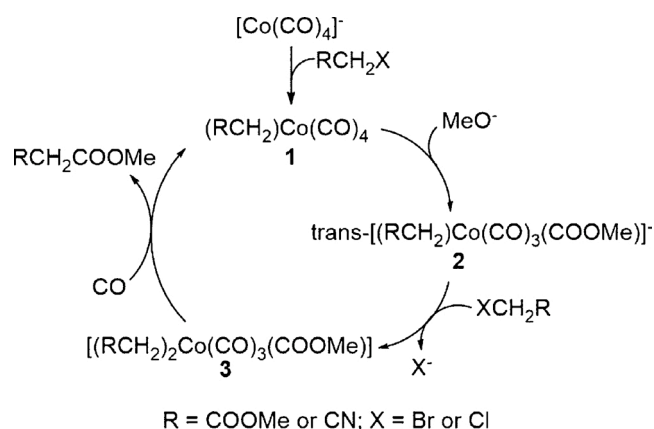
E-mail addresses: shenchaoren@gmail.com (C. Shen), tianxx@sxu.edu.cn (X. Tian).

<https://doi.org/10.1016/j.mcat.2020.111237>

Received 29 August 2020; Received in revised form 26 September 2020; Accepted 28 September 2020

Available online 9 October 2020

2468-8231/© 2020 Elsevier B.V. All rights reserved.

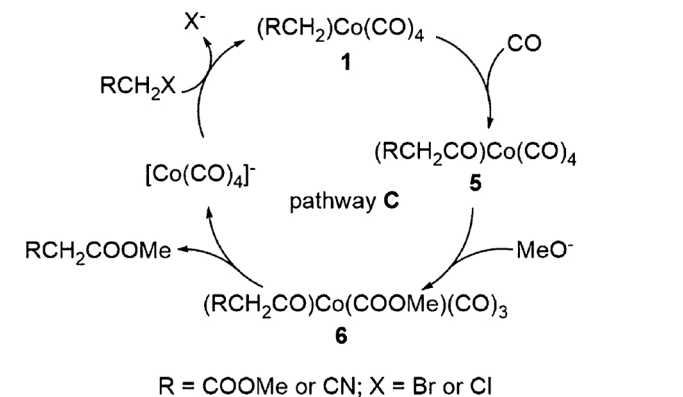
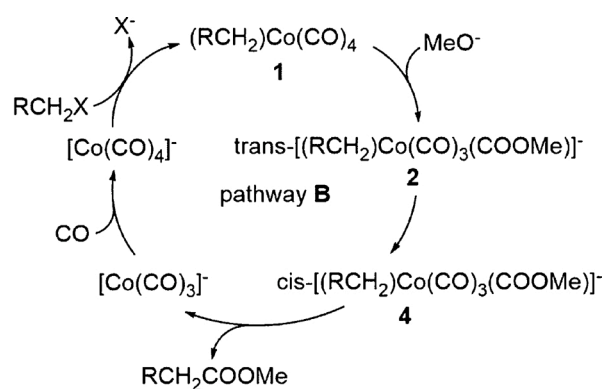


Scheme 1. The proposed mechanism (pathway A) of cobalt-catalysed methoxycarbonylation of alkyl halides based on $(RCH_2)Co(CO)_4$ as the active catalytic species.

infrared spectroscopy, nuclear magnetic resonance spectroscopy and extend X-ray absorption fine structure (EXAFS) [20,21]. In this catalytic cycle, $(RCH_2)Co(CO)_4$ (1) was regarded as the active catalytic species. Considering the fact that $[Co(CO)_4]^-$ is usually employed as the pre-catalyst, the formation of 1 was through the S_N2 reaction between $[Co(CO)_4]^-$ and alkyl halide. Via the nucleophilic attack of methoxide anion on the carbonyl ligand of 1, the anionic complex $trans-[(RCH_2)Co(CO)_3(COOMe)]^-$ (2) was formed. Afterwards, the S_N2 reaction between 2 and alkyl halide substrate proceeded and afforded the neutral six-coordinated cobalt complex $[(RCH_2)_2Co(COOMe)(CO)_3]$ (3). The following reductive elimination released free RCH_2COOMe and regenerate the cobalt-alkyl complex 1. To the best of our knowledge, the transformation from 2 to 3 and the regeneration of 1 from 3 was yet to be verified by experimental evidence. More than the mechanism illustrated in *scheme 1* (pathway A), here we proposed other two plausible reaction pathways (*Scheme 2*). Also assuming $(RCH_2)Co(CO)_4$ as the active catalytic species, the pathway B went through the isomerization of 2 to its cis-isomer 4, the reductive elimination of 4 and the recovery of $[Co(CO)_4]^-$. the pathway C went directly to the carbonylation of 1 to cobalt acyl complex (5), and further methanolysis of 5. The reaction pathways were evaluated from the perspective of thermodynamics. Since $Na[Co(CO)_4]$ and $MeONa$ were used in the previous experimental investigations [12,15], we also compared the results of computational models with and without sodium counteraction. The detailed results of considering sodium counteraction on the thermodynamics properties see Table S2 in Supplementary Material.

Computational method

All DFT calculations were performed using Gaussian 16 program [29]. Considering the applicability of M06 hybrid meta exchange-correlation functional on homogeneous organometallic thermochemistry [30,31], geometries were optimized and characterized by frequency calculations to be local minima or transition states (TS) at the M06/BS level in gas phase, BS designating a mixed basis set of SDD for Br and Co atoms [32,33], and 6-311+G(d) for other atoms. The free energies (kcal/mol) at 298 K and 1 atm were generally used in the following discussions. Intrinsic reaction coordinate calculations were also conducted to confirm that each transition state connects two relevant minima. Since either the corresponding polar alcohol substrate (e.g. MeOH) or the carboxylic ester product (e.g. $CH_2(COOMe)_2$) can be employed as the solvent in the cobalt-catalysed alkoxy carbonylation of alkyl halides [18,19], the nonspecific solvation effects of MeOH ($\epsilon = 32.613$) and $CH_2(COOMe)_2$ ($\epsilon = 10.4$) were considered by calculating single-point energies with the gas-phase optimized geometries [34] in the IEFPCM model [35] at the same level. The solvation effects of MeOH



Scheme 2. The other two plausible reaction pathways (pathway B and C) based on $[Co(CO)_4]^-$ as the active catalytic species.

in the IEFPCM model were qualitatively consistent with that obtained in the SMD model [36] (detailed results see Supplementary Material). This test indirectly validated the reliability of $CH_2(COOMe)_2$ solvation effects which were calculated by IEFPCM model. Natural Bond Orbital (NBO) population analysis was performed for the calculation of natural atomic charges [37].

The following notations are employed. A, B and C respectively represent the pathway A, B and C. The subscripts respectively represent the following transformation: i) **SN2** refers to S_N2 reaction; ii) **iso** refers to isomerization; iii) **eliminate** refers to reductive elimination; iv) **insert** refers to migratory CO insertion; v) **CO** refers to CO coordination to cobalt center. ΔG_A and ΔG_R represent the activation free energy and reaction free energy of elementary step, respectively. The values in the first and second parentheses of Tables 1–8 are the free energies after considering MeOH and $CH_2(COOMe)_2$ solvation effect, respectively.

Table 1
 S_N2 reaction of $[Co(CO)_4]^-$ with electrophilic alkyl halides.

R	X	ΔG_A	ΔG_R
CN	Br	10.7 (16.5)	-3.9 (-2.4)
COOMe	Br	14.2 (17.5) (17.6)	8.1 (0.8) (-1.9)
COOMe	Cl	22.5 (24.0) (24.1)	16.4 (5.4) (7.2)
Cl	Cl	27.3 (27.5)	9.9 (5.5)

Table 2
The addition of methoxide anion onto the carbonyl ligand of complex 1.

	$\Delta G_R(2)$	$\Delta G_R(4)$
COOMe	-55.3 (-25.4) (-27.7)	-47.5 (-18.0) (-20.2)
CN	-61.0 (-28.2)	-54.0 (-20.8)

Table 3
 S_N2 reaction of alkyl halides with $\text{trans-}[(\text{RCH}_2)\text{Co}(\text{CO})_3(\text{COOMe})]^-$ anion.

	X	ΔG_A	ΔG_R
COOMe	Br	18.2 (21.7) (21.7)	12.5 (9.0) (6.1)
	Cl	27.2 (27.8) (27.9)	22.7 (13.5) (15.2)
CN	Br	18.7 (22.9)	7.7 (9.9)

Table 4
Reductive elimination of complex 3 to release product and regenerate $(\text{RCH}_2)\text{Co}(\text{CO})_4$.

	ΔG_{A1}	ΔG_{R1}	ΔG_{R2}
COOMe	19.7 (19.1) (19.3)	-34.1 (-37.0) (-36.6)	-7.6 (-7.1) (-7.2)
CN	20.0 (19.3)	-33.7 (-35.7)	-6.7 (-7.4)

Results and discussion

The reaction pathways A, B and C for the carbonylation of EWG-activated alkyl halides are all initiated with the S_N2 reaction between nucleophilic $[\text{Co}(\text{CO})_4]^-$ and electrophilic alkyl halides. Similar S_N2 reaction between CH_3I and $[\text{Rh}(\text{CO})_2\text{L}_2]^-$ has been thoroughly investigated in the carbonylation of methanol by means of DFT calculation without considering counteraction [38,39]. However, to the best of our

knowledge, there was lack of relevant theoretical investigation on the reaction between $[\text{Co}(\text{CO})_4]^-$ and alkyl halide. Herein, BrCH_2CN , XCH_2COOMe ($\text{X} = \text{Br}$ or Cl) and CH_2Cl_2 were selected as the models of alkyl halide substrate to investigate this elementary step.

As shown in Table 1, BrCH_2CN is the most reactive substrate among these four model substrates, possessing the lowest activation energy (10.7 kcal/mol) and exothermic reaction feature (-3.9 kcal/mol). The reaction for XCH_2COOMe substrate is endothermic, except for

Table 5
Isomerization of 2 to 4 via pseudorotation.

	ΔG_A	ΔG_R
COOMe	14.2(13.3) (13.5)	7.8 (7.5) (7.5)
CN	15.6 (13.7)	7.0 (7.4)

Table 6
Reductive elimination of **4** to release product and regenerate $[\text{Co}(\text{CO})_4]^-$.

	ΔG_{A1}	ΔG_{R1}	ΔG_{R2}
COOMe	15.2 (15.2) (15.3)	-9.3 (-16.4) (-15.9)	-30.4 (-27.1) (-27.3)
CN	18.2 (17.1)	-0.6 (-11.1)	

$\text{BrCH}_2\text{COOMe}$ in the solvation of $\text{CH}_2(\text{COOMe})_2$. And the reaction of chloride is more endothermic than that of bromide (16.4 vs. 8.1 kcal/mol). The energy barrier of chloride is also higher than that of bromide (22.5 vs. 14.2 kcal/mol). The reaction of CH_2Cl_2 with $[\text{Co}(\text{CO})_4]^-$ not only is endothermic (9.9 kcal/mol) but also has the highest energy barrier of 27.3 kcal/mol. It is noteworthy that the free-energy changes in the gas-phase is obtained from X^- -associated complex **1** rather than the isolated **1** and X^- as the final state. The reason for this choice is the well-known charge redistribution effect, which makes the reaction energy exaggerated positive. In the obtained final-state complex, there is weak electrostatic interaction between the halide anion and the carbonyl ligand of $(\text{RCH}_2)\text{Co}(\text{CO})_4$, which subtly changes the configuration of the complex, especially the location of halide anion. This is indicated by NBO analysis (detailed structures and results of natural atomic charges see Supplementary Material). Solvation of MeOH or $\text{CH}_2(\text{COOMe})_2$ makes the reaction more thermodynamically favoured, even when the isolated **1** and X^- are employed as the final state (Table 1), which fits the experimental cryogenic conditions well. However, the solvation elevates the energy barrier to a certain degree. Based on the above results, the consideration of solvation effect is indispensable to get a relatively rational energetic profile.

When Na^+ is taken into account, the thermodynamic contribution of producing NaX salt turns this $\text{S}_{\text{N}}2$ reaction to be much more exoergic for all four model substrates (detailed results see Table S2 in Supplementary Material). Meanwhile, the solvation both drastically increases the activation energy and makes the reaction more thermodynamically beneficial. Considering the MeOH solvation effect, BrCH_2CN still possesses the lowest activation energy (15.9 kcal/mol), while CH_2Cl_2 has the highest barrier (36.5 kcal/mol). XCH_2COOMe have moderate activation energies and $\text{BrCH}_2\text{COOMe}$ remains more reactive than $\text{ClCH}_2\text{COOMe}$

(21.0 vs. 27.7 kcal/mol). Therefore, we can deduce that CH_2Cl_2 is much less reactive than both BrCH_2CN and XCH_2COOMe , when $[\text{Co}(\text{CO})_4]^-$ is utilized. This pattern is consistent with the previous experimental report that $[\text{Co}(\text{CO})_4]^-$ is not very efficient for the alkoxycarbonylation of CH_2Cl_2 [28]. Therefore, no further calculation was considered based on CH_2Cl_2 .

After the $\text{S}_{\text{N}}2$ reaction, the generated $(\text{RCH}_2)\text{Co}(\text{CO})_4$ (**1**) has two alternative transformation pathways: i) further conversion to $[(\text{RCH}_2)\text{Co}(\text{CO})_3(\text{COOMe})]^-$ via the nucleophilic addition of methoxide anion onto the carbonyl ligand of complex **1** (pathway A or B); ii) undergoing migratory CO insertion to form acetyl cobalt complex $(\text{RCH}_2\text{CO})\text{Co}(\text{CO})_4$ (pathway C). Based on these two different options, the mechanism of pathway A, B and C is discussed respectively in the following text.

Pathway A

Regarding the generation of anionic complex **2**, as shown in Table 2, the transformation from complex **1** to **2** via the addition of methoxide anion onto the axial cobalt-coordinated carbonyl ligand is strongly exothermic (-55.3 and -61.0 kcal/mol) without evident energy barrier, although the solvation of MeOH or $\text{CH}_2(\text{COOMe})_2$ drastically diminishes the exothermic trait of this nucleophilic addition step. For both $(\text{MeOOCCH}_2)\text{Co}(\text{CO})_4$ and $(\text{NCCH}_2)\text{Co}(\text{CO})_4$, the nucleophilic addition onto the axial carbonyl ligand (**2**) is more exothermic than the equatorial carbonyl ligand (**4**).

When considering the sodium countercation, there is no evident preference between forming **2** and **4** with or without solvation effect, albeit the solvation of MeOH or $\text{CH}_2(\text{COOMe})_2$ drastically diminishes the exothermic trait of this nucleophilic addition step (detailed results see Table S2 in Supplementary Material). It should be mentioned that

Table 7
Migratory CO insertion and following CO addition in pathway C.

	ΔG_A	ΔG_R
COOMe	12.4 (11.4) (11.5)	8.9 (7.4) (7.6)
CN	14.5 (14.0)	13.1 (11.5)

	ΔG_A	ΔG_R
COOMe	9.4 (8.8) (8.9)	-6.8 (-6.6) (-6.6)
CN	6.3 (5.2)	-9.0 (-9.0)

unlike the tetrameric or hexameric aggregation of alkali metal tert-butoxides [40], the unsolvated MeONa has layered structure [40,41]. Therefore, when sodium counteraction is taken into the consideration of computational model, the monomeric MeONa is adopted. Moreover, the infrared spectrum of $\text{trans}-(\text{MeOOCCH}_2)\text{Co}(\text{CO})_3(\text{CO}_2\text{Me})^-$ estimated by DFT computation fits well with the data reported in the literatures (Detailed comparisons see Supplementary Material) [15].

After generating **2**, the previously proposed mechanism suggested the $\text{S}_{\text{N}}2$ reaction of **2** with XCH_2R to afford higher-valent neutral $[(\text{RCH}_2)_2\text{Co}(\text{CO})_3(\text{COOMe})]$ complex (**3**). Table 3 exhibits the barrier and reaction energy for this step.

It is shown that the reaction is endothermic for all three substrates. For $\text{BrCH}_2\text{COOMe}$, the $\text{S}_{\text{N}}2$ reaction is endothermic with an energy barrier of 18.2 kcal/mol. Switching to $\text{ClCH}_2\text{COOMe}$, the $\text{S}_{\text{N}}2$ reaction turns to be even more endothermic with higher activation energy (27.2 kcal/mol). In comparison with $\text{BrCH}_2\text{COOMe}$, the reaction of BrCH_2CN needs to overcome similar energy barrier (18.7 kcal/mol), but the reaction is much less endothermic. Including solvation effect, $\text{BrCH}_2\text{COOMe}$ still has comparable barrier and reaction energy with that of BrCH_2CN , the reaction of chloride $\text{ClCH}_2\text{COOMe}$ is less favoured both kinetically and thermodynamically than the two bromide. In the Na^+ -present circumstance, similar reaction preference between the chloride and the two bromides was obtained. The energy barriers even close to the corresponding energy barriers without sodium counteraction when including solvation effect. And once again, the presence of counteraction turns the endergonic reaction into exergonic process, but only within the consideration of solvation effect. More detailed relevant results see Table S2 in Supplementary Material.

The subsequent reductive elimination of **3** to release the carbonylation product as well as regenerate the active $(\text{RCH}_2)\text{Co}(\text{CO})_4$. Table 4 displays the energy patterns of these steps. The reductive elimination of $[(\text{RCH}_2)_2\text{Co}(\text{CO})_3(\text{COOMe})]$ ($\text{R} = \text{COOMe}$ or CN) is strongly exothermic with the energy barrier of about 20 kcal/mol. The following addition of CO onto $(\text{RCH}_2)\text{Co}(\text{CO})_3$ to recover $(\text{RCH}_2)\text{Co}(\text{CO})_4$ are both exothermic. The impact of solvation on the reductive elimination is about 1 kcal/mol.

Pathway B

In pathway B, complex **4** affords RCH_2COOMe and $[\text{Co}(\text{CO})_3]^-$ by reductive elimination. In the model of considering sodium counteraction, the formation of **4** directly from nucleophilic addition of MeO^- on complex **1** is competitive with the formation of **2** (see Table S2 in

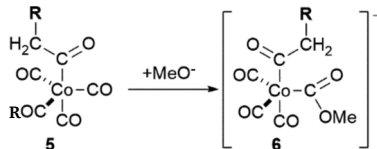
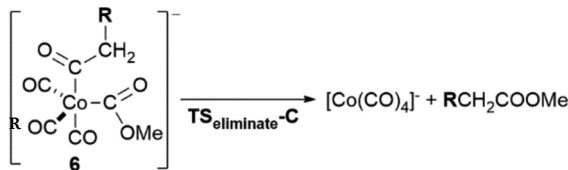
Supplementary Material). However, complex **2** is thermodynamically more favoured than complex **4** in the Na^+ -absent model. Given the inconsistency between the two models and the previous characterization results [21], the isomerization from **2** to **4** is considered. Theoretically, there are two plausible routes for the isomerization of **2** to **4**: i) the intramolecular migration of methoxy group; ii) the Berry-type pseudorotation of **2** [42–44]. The computational results display that the energy barrier for pseudorotation is much lower than for the intramolecular migration of methoxy group (detailed comparison of two routes see Table S1 in Supplementary Material). As shown in Table 5, the pseudorotation isomerization barriers of anionic **2** to **4** are about 15 kcal/mol, and were slightly reduced in the solvation of MeOH or $\text{CH}_2(\text{COOMe})_2$. When considering sodium counteraction, the energy barriers for pseudorotation were further turned down to 5–7 kcal/mol (the corresponding results see Table S2 in Supplementary Material). Obviously, the barrier is considerably low and the isomerization between **2** and **4** is easy to proceed.

The energy patterns of reductive elimination are listed in Table 6. In comparison with the reductive elimination of complex **3**, although the reductive elimination of **4** to $[\text{Co}(\text{CO})_3]^-$ has a slightly lower energy barrier, the reaction is much less exothermic. Recovering $[\text{Co}(\text{CO})_4]^-$ by the CO addition onto $[\text{Co}(\text{CO})_3]^-$ is a strongly exothermic reaction. It should be mentioned that, with considering the solvation of MeOH or $\text{CH}_2(\text{COOMe})_2$, the transformation process from **4** to $[\text{Co}(\text{CO})_3]^-$ become more exothermic but less exothermic for the CO addition step. The solvation effect on reaction energy is more remarkable when considering the counteraction.

Pathway C

In pathway C, the transformation from **1** to **5** by CO insertion undergoes two steps (Table 7). The first step, migratory CO insertion of **1** to afford $(\eta^2\text{-RCH}_2\text{CO})\text{Co}(\text{CO})_3$ ($(\text{RCH}_2\text{CO})\text{Co}(\text{CO})_3$, $\text{R} = \text{CN}$ or COOMe), is an endothermic reaction. In $(\eta^2\text{-RCH}_2\text{CO})\text{Co}(\text{CO})_3$ complex, there is an additional $\text{Co}\cdots\text{H}-\text{C}$ agostic interaction at the formally vacant equatorial position. There are two potential accesses for the subsequent CO addition on $(\text{RCH}_2\text{CO})\text{Co}(\text{CO})_3$, one is via the rotation of acyl group (i.e. the $\text{Co}\cdots\text{H}-\text{C}$ agostic interaction of complex $(\text{RCH}_2\text{CO})\text{Co}(\text{CO})_3$ is transformed to the $\text{Co}\cdots\text{O}=\text{C}$ agostic interaction) followed by the CO addition; the other is via the direct CO addition on to $(\text{RCH}_2\text{CO})\text{Co}(\text{CO})_3$ by breaking the $\text{Co}\cdots\text{H}-\text{C}$ agostic interaction. The computational results suggest that the direct CO addition onto $(\text{RCH}_2\text{CO})\text{Co}(\text{CO})_3$ is more viable because of its lower energy barrier (detailed comparison see

Table 8
The methanolysis of $(\text{RCH}_2\text{CO})\text{Co}(\text{CO})_4$.

		
		ΔG_{R}
COOMe		–51.6 (–20.8) (–23.0)
CN		–58.6 (–22.4)
		
		ΔG_{A}
COOMe	27.0 (28.0) (27.9)	ΔG_{R}
CN	26.6 (26.6)	–37.6 (–41.5) (–41.3)
		–30.5 (–39.2)

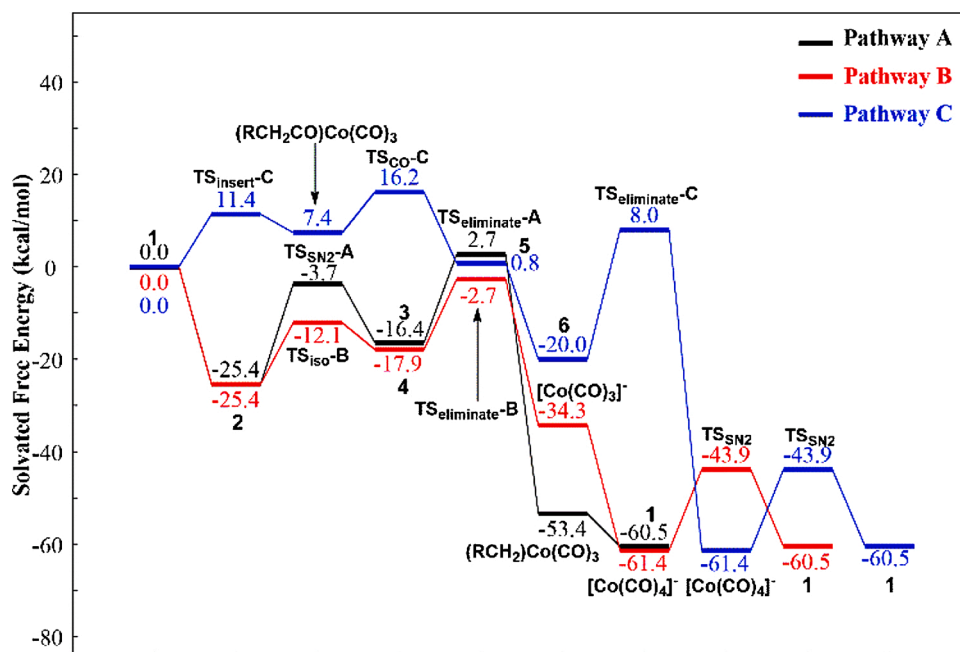


Fig. 1. PES of cobalt-catalysed methoxycarbonylation of $\text{BrCH}_2\text{COOMe}$ with the solvation of MeOH for pathway A (black), pathway B (red) and pathway C (blue) without considering the presence of Na^+ .

Table 9

The methoxylation of XCH_2COOMe to $\text{MeOCH}_2\text{COOMe}$ in the solvation of MeOH .

	ΔG_{R1}	ΔG_{A2}	ΔG_{R1}
Br	-4.2	6.6	-37.1
Cl	-3.1	10.2	-33.6

Table S1 and S2 in Supplementary Material). This step is exoergic but cannot offset the energy demand in last CO migration step. The solvation of MeOH or $\text{CH}_2(\text{COOMe})_2$ has minor affect to the energy barrier and reaction free-energy change of both two steps.

As the terminal step in pathway C, three different pathways regarding the methanolysis of $(\text{RCH}_2\text{CO})\text{Co}(\text{CO})_4$ (5) have been proposed in the literature [45]: i) the elimination of ketene; ii) the nucleophilic additional of methoxide anion onto the carbon atom of coordinated CO ligand and subsequent migration of methoxy group from the equatorial position to the acyl group; iii) the direct nucleophilic attack of methoxide anion onto the positively charged carbon atom of acyl carbonyl in $(\text{RCH}_2\text{CO})\text{Co}(\text{CO})_4$. The first scenario has been definitely excluded by experimental evidence. Although Sóvágó et al. regarded the third scenario as the most probable pathway, they also mentioned that the second scenario has already been established as the source of various $[\text{XYCo}(\text{CO})_3]^-$ complexes, where X and Y are an alkyl, alkoxy, acyl or alkoxyacyl group [20,46]. In this study, we failed to locate the corresponding transition states for the methanolysis via the direct attack of methoxide anion on the acyl group of $(\text{RCH}_2\text{CO})\text{Co}(\text{CO})_4$ ($\text{R}=\text{CN}$ or COOMe). However, the transition states of the addition of methoxide anion onto the carbon atom of coordinated carbonyl group at the equatorial site ($5 \rightarrow 6$), and the transition states of the migration of methoxy group from the equatorial carbonyl to the acetyl group ($6 \rightarrow [\text{Co}(\text{CO})_4]^- + \text{RCH}_2\text{COOMe}$) which included in the second scenario were

both located. NBO analysis reveals that in intermediate 5, the carbon atoms of coordinated CO ligands are more positively-charged than the carbon atom of RCH_2CO acyl group (detailed results about the natural atomic charges obtained by NBO analysis see Supplementary Material). This implies that the addition of methoxide anion onto the carbon atom of coordinated carbonyl group in intermediate 5 should have precedence over the direct nucleophilic attack of MeO^- onto the acyl carbonyl of $(\text{RCH}_2\text{CO})\text{Co}(\text{CO})_4$. This two-step methanolysis reaction mode was also found in the reductive elimination of dimethylcarbonate from $[(\text{MeOOC})_2\text{Co}(\text{CO})_3]^-$ [47]. Table 8 exhibits the energy barriers and free-energy changes of these two steps. For the addition of methoxide anion, no evident energy barrier is found, but the migration of methoxy group has to overcome an energy barrier over 25 kcal/mol. This value is close to the literature-reported ΔH^\ddagger for methanolysis of $(\text{MeCO})\text{Co}(\text{CO})_4$ in methanol solution [45]. This consistence also verifies the rationality of the second scenario in some extent. Therefore, only the pathway of second scenario is discussed in the following part. Both steps in Table 8 are strongly exothermic. Interestingly, the reaction energy of the former step becomes much less exothermic in the consideration of solvation effect, while that of the latter step turns to be more exothermic. When Na^+ is considered into the model, the addition of MeONa onto the carbonyl ligand turns to be less exothermic. The energy barrier for the following migration of methoxy group from the equatorial position to the acetyl group ($6 \rightarrow \text{Na}[\text{Co}(\text{CO})_4]^- + \text{RCH}_2\text{COOMe}$) was significantly

higher than the Na⁺-absent scenario even when the solvation is considered (detailed results see Table S2 in Supplementary Material).

Potential energy profiles of three reaction pathways

Based on the above-mentioned computational results, pathways **A**, **B** and **C** were compared from the perspective of thermodynamics.

As the catalytic cycle starts off and ends with complex **1**, a complete circle from **1** to **1** was described in the diagram of potential energy surface (PES). BrCH₂COOMe substrate is taken for instance. As shown in Fig. 1, the overall methoxycarbonylation reaction is highly exothermic by 60.5 kcal/mol, and pathway **C** possesses considerably higher transition state energy (TS_{Co-C}) than Pathway **A** and **B**, therefore is unfavoured. According to the energetic span theory [48], the TOF-determining transition states (TDTS) in pathway **A** and **B** are both TS_{eliminate}, and the TOF-determining intermediates (TDI) are both intermediate **2**. The corresponding energetic span (ΔE) for pathway **A** and **B** are 28.1 and 22.7 kcal/mol, respectively. Apparently, pathway **B** is kinetically more favoured than pathway **A** due to the lower energy span.

It should be noted that even for the critical divergent elementary step (2 → 3/4 in pathway **A/B**), the reaction barrier in pathway **A** is 8.4 kcal/mol higher than that of in pathway **B**. The results suggest that the formation of intermediate **3** is much less probable. Therefore, the simultaneous formation of two different esters when adding BrCH₂CN and BrCH₂COOMe substrates into the methanolic solution of (NCCH₂)Co(CO)₄ at the same time [20], could be just ascribed to the swift transferring of different alkyl groups from RCH₂X onto the recovered [Co(CO)₄]⁻ during the catalytic cycle in pathway **B**.

Furthermore, the presence of counteraction indeed changes the PES shape, especially the thermodynamics properties of elementary steps, but the relatively preference of different pathways in this reaction remains same (detailed results see Fig. S16 in Supplementary Material).

The PES for the methoxycarbonylation of BrCH₂CN and XCH₂COOMe (X = Cl or Br) with or without considering the solvation and sodium counteraction see Figs. S1–21 in Supplementary Material. Similar conclusion could also be obtained.

Methoxylation: one of the plausible side reactions

The methoxylation of XCH₂COOMe (MeO⁻ + XCH₂COOMe → X⁻ + MeOCH₂COOMe) is one of the potential undesired side reactions during the cobalt-catalysed methoxycarbonylation. This side reaction firstly undergoes the formation of ion-molecule complex [49] between methoxide anion and XCH₂COOMe. Subsequently, the reactant complex goes through an intramolecular S_N2-type substitution to generate halide anion and MeOCH₂COOMe. We also took Na⁺ as the counteraction to investigate the side reaction. The computational results indicate that the presence of counteraction largely changes the reaction energy profile. In the absence of sodium counteraction (Table 9), the formation of ion-molecule complex between MeO⁻ and XCH₂COOMe is exergonic. Considering the presence of sodium counteraction turns this step to be endergonic (Table S4). In the following intramolecular S_N2-type substitution, the energy barrier of considering the contribution of Na⁺ is higher than in the absence of Na⁺ by more than 5.0 kcal/mol, but the reaction is more exothermic in the presence of Na⁺ (detailed results see Table S4 in Supplementary Material).

For BrCH₂COOMe in the solvation of MeOH, as instance, the methoxylation barrier is 2.4 or 14.4 kcal/mol without or with the counteraction, higher than that of methoxycarbonylation (-2.7/4.9 kcal/mol). The results suggest that the interference from methoxylation during the methoxycarbonylation of BrCH₂COOMe is minor. This pattern is also established in the methoxycarbonylation of ClCH₂COOMe. More detailed results regarding the energy profiles for the methoxylation of XCH₂COOMe in gas phase or considering the solvation of dimethyl malonate see Table S3, S4 and Fig S23–26 in

Supplementary Material.

Conclusions

In summary, the mechanism of cobalt-catalysed alkoxy carbonylation of alkyl halides bearing strong electron-withdrawing group have been discussed by computationally investigating the methoxycarbonylation of BrCH₂CN and XCH₂COOMe (X = Br or Cl) with the consideration of solvation. Three different reaction pathways were compared. Pathway **B**, which goes through the addition of MeO⁻ to (RCH₂)Co(CO)₄ and the elimination of [(RCH₂)Co(CO)₃(COOMe)]⁻ to afford ester was found to be the most kinetically favoured. However, the previously proposed pathway **A**, which needs to go through the S_N2 reaction of XCH₂R with [(RCH₂)Co(CO)₃(COOMe)]⁻, has 5.4 kcal/mol higher energy span than pathway **B**, therefore it is unfavoured. Pathway **C** through directly carbonylation of (RCH₂)Co(CO)₄ and further methanolysis of (RCH₂CO)Co(CO)₄ is the least favoured due to the highest barrier.

The catalytic process is initiated with the formation of (RCH₂)Co(CO)₄ via the S_N2 reaction of RCH₂X with [Co(CO)₄]⁻. Among the studied substrates, CH₂Cl₂ is ruled out because of the considerably high initiation barrier. BrCH₂CN is more reactive than XCH₂COOMe (X = Cl or Br), and BrCH₂COOMe is more reactive than ClCH₂COOMe to form the active species (RCH₂)Co(CO)₄ of catalytic cycle.

Furthermore, the importance of sodium counteraction was evaluated. The presence of counteraction in the model indeed changes the PES shape, especially reshapes the thermodynamics trait of elementary steps, meanwhile the relatively preference of different pathways is retained.

CRediT authorship contribution statement

Yanwei Cao: Investigation. **Chaoren Shen:** Investigation, Writing - original draft. **Jie Min:** Investigation, Visualization. **Lin He:** Project administration, Funding acquisition. **Xinxin Tian:** Project administration, Writing - review & editing, Supervision.

Declaration of Competing Interest

There are no conflicts to declare.

Acknowledgements

The work was financially supported by the National Natural Science Foundation of China (No. 21903049 and U1510103 for X.T., 21802151 for C.S., 91645118 and 21633013 for L.H.) and Key Research Program of Frontier Sciences of CAS (QYZDJ-SSW-SLH051). Part of the calculations were performed at the Shanghai Supercomputing Centre and the Supercomputing Centre of Shanxi University.

Appendix A. Supplementary data

Supplementary material related to this article can be found, in the online version, at doi:<https://doi.org/10.1016/j.mcat.2020.111237>.

References

- [1] M. Beller, *Catalytic Carbonylation Reactions*, Springer Verlag, Berlin-Heidelberg, 2006.
- [2] X.-F. Wu, M. Beller, *Transition Metal Catalyzed Carbonylation Reactions*, Springer Verlag, Berlin-Heidelberg, 2013.
- [3] X.-F. Wu, M. Beller, *Transition Metal Catalyzed Carbonylative Synthesis of Heterocycles*, Springer Verlag, Berlin-Heidelberg, 2015.
- [4] J. Hartwig, *Organotransition Metal Chemistry: From Bonding to Catalysis*, University Science Books, Sausalito, 2010, pp. 301–320.
- [5] B.T. Sargent, E.J. Alexanian, *J. Am. Chem. Soc.* 138 (2016) 7520–7523.
- [6] H.M. Colquhoun, D.J. Thompson, M.V. Twigg, in *Carbonylation: Direct Synthesis of Carbonyl Compounds*, Springer US, New York, 1991, p. 111, ch. 7.
- [7] R.F. Heck, D.S. Breslow, *J. Am. Chem. Soc.* 85 (1963) 2779–2782.
- [8] S. Gobölös, E. Tálas, J. Margitfalvi, *Stud. Surf. Sci. Catal.* 41 (1988) 337–344.

- [9] J. Hu, Q. Zhang, Z. Guan, Y. Gu, W. Mo, T. Li, G. Li, *ChemCatChem* 4 (2012) 1776–1782.
- [10] Y. Lei, R. Zhang, L. Wu, Q. Ou, H. Mei, G. Li, *J. Mol. Catal. A Chem.* 392 (2017) 105–111.
- [11] Y. Wan, Z. Chen, D. Liu, Y. Lei, *Catalysts* 8 (2018) 586.
- [12] M. Foà, F. Francalanci, G. Cainelli, A. Umami-Ronchi, *J. Organomet. Chem.* 248 (1983) 225–231.
- [13] M. Foà, F. Francalanci, *J. Mol. Catal.* 41 (1987) 89–107.
- [14] M.L. Kantam, N.P. Reddy, B.M. Choudary, *Synth. Commun.* 20 (1990) 31–2640.
- [15] F. Ramirez-Vega, P. Laurent, J.-C. Clément, H. des Abbayes, *J. Mol. Catal. A Chem.* 96 (1995) 15–20.
- [16] Z. Hao, X. Jiang, *Chin. J. Catal.* 25 (2004) 257–258.
- [17] W.-J. Jiang, W.-L. Mo, Y.-M. Jia, G.-X. Li, *Chem. J. Chin. Univ.* 33 (2012) 373–377.
- [18] H. Strittmatter, S. Hildbrand, P. Pollak, *Malonic Acid and Derivatives in Ullmann's Encyclopedia of Industrial Chemistry*, Wiley-VCH, Weinheim, 2007.
- [19] H.A. Wittcoff, B.G. Reuben, J.S. Plotkin, *Industrial Organic Chemicals*, 3rd edn, John Wiley & Sons, Hoboken, 2012, p. 457, ch. 12.
- [20] F. Francalanci, A. Gardano, L. Abis, M. Foà, *J. Organomet. Chem.* 251 (1983) C5–C8.
- [21] G. Vlaic, J.C.J. Bart, M. Foà, F. Francalanci, R. Clement, *J. Organomet. Chem.* 287 (1985) 369–375.
- [22] N. Argaman, G. Makov, *Am. J. Phys.* 68 (2000) 69–79.
- [23] D. Sholl, J.A. Steckel, *Density Functional Theory: A Practical Introduction*, John Wiley & Sons, Hoboken, 2009.
- [24] J.N. Harvey, *Annu. Rep. Prog. Chem., Sect. C: Phys. Chem.* 102 (2006) 203–226.
- [25] T. Sperger, I.A. Sanhueza, I. Kalvet, F. Schoenebeck, *Chem. Rev.* 115 (2015) 9532–9586.
- [26] V.P. Ananikov, *Understanding Organometallic Reaction Mechanisms and Catalysis: Computational and Experimental Tools*, Wiley-VCH, Weinheim, 2014.
- [27] G.-J. Cheng, X. Zhang, L.W. Chung, L. Xu, Y.-D. Wu, *J. Am. Chem. Soc.* 137 (2015) 1706–1725.
- [28] P. Suisse, S. Pellegrini, Y. Castanet, A. Mortreux, S. Lecolier, *J. Chem. Soc. Chem. Commun.* (1995) 847–848.
- [29] M.J. Frisch, G.W. Trucks, H.B. Schlegel, G.E. Scuseria, M.A. Robb, J.R. Cheeseman, G. Scalmani, V. Barone, G.A. Petersson, H. Nakatsuji, X. Li, M. Caricato, A. V. Marenich, J. Bloino, B.G. Janesko, R. Gomperts, B. Mennucci, H.P. Hratchian, J. V. Ortiz, A.F. Izmaylov, J.L. Sonnenberg, D. Williams-Young, F. Ding, F. Lipparini, F. Egidi, J. Goings, B. Peng, A. Petrone, T. Henderson, D. Ranasinghe, V. G. Zakrzewski, J. Gao, N. Rega, G. Zheng, W. Liang, M. Hada, M. Ehara, K. Toyota, R. Fukuda, J. Hasegawa, M. Ishida, T. Nakajima, Y. Honda, O. Kitao, H. Nakai, T. Vreven, K. Throssell, J.A. Montgomery Jr., J.E. Peralta, F. Ogliaro, M. J. Bearpark, J.J. Heyd, E.N. Brothers, K.N. Kudin, V.N. Staroverov, T.A. Keith, R. Kobayashi, J. Normand, K. Raghavachari, A.P. Rendell, J.C. Burant, S.S. Iyengar, J. Tomasi, M. Cossi, J.M. Millam, M. Klene, C. Adamo, R. Cammi, J.W. Ochterski, R.L. Martin, K. Morokuma, O. Farkas, J.B. Foresman, D.J. Fox, *Gaussian 16*, Revision A.03.03, Gaussian, Inc., Wallingford C.T., 2016.
- [30] Y. Zhao, D. Truhlar, *Acc. Chem. Res.* 41 (2008) 157–167.
- [31] Y. Zhao, D. Truhlar, *Theor. Chem. Acc.* 120 (2008) 215–241.
- [32] M. Dolg, U. Wedig, H. Stoll, H. Preuss, *J. Chem. Phys.* 86 (1987) 866–872.
- [33] D. Andrae, U. Haussermann, M. Dolg, H. Stoll, H. Preuss, *Theor. Chem. Acc.* 77 (1990) 123–141.
- [34] R.F. Ribeiro, A.V. Marenich, C.J. Cramer, D.G. Truhlar, *J. Phys. Chem. B* 115 (2011) 14556–14562.
- [35] J. Tomasi, B. Mennucci, R. Cammi, *Chem. Rev.* 105 (2005) 2999–3093.
- [36] A.V. Marenich, C.J. Cramer, D.G. Truhlar, *J. Phys. Chem. B* 113 (2009) 6378–6396.
- [37] E.D. Glendening, C.R. Landis, F. Weinhold, *J. Comput. Chem.* 34 (2013) 1429–1437.
- [38] T.R. Griffin, D.B. Cook, A. Haynes, J.M. Pearson, D. Monti, G.E. Morris, *J. Am. Chem. Soc.* 118 (1996) 3029–3030.
- [39] M. Feliz, Z. Freixa, P.W.N.M. van Leeuwen, C. Bo, *Organometallics* 24 (2005), 5718–572.
- [40] E. Weiss, *Angew. Chem. Int. Ed. Engl.* 32 (1993) 1501–1670.
- [41] E. Weiss, *Z. Anorg. Allg. Chem.* 332 (1964) 197–203.
- [42] R.S. Berry, *J. Chem. Phys.* 32 (1960) 933–938.
- [43] H.L. Strauss, *Ann. Rev. Phys. Chem.* 34 (1983) 301–328.
- [44] M.E. Cass, K.K. Hii, H.S. Rzepa, *J. Chem. Educ.* 83 (2006) 336.
- [45] J. Sóvágó, A. Sisak, F. Ungváry, L. Markó, *Inorg. Chim. Acta* 227 (1994) 297–300.
- [46] M. Tasi, G. Pályi, *Organometallics* 4 (1985) 1523–1528.
- [47] G. Fachinetti, T. Funaioli, D. Masi, C. Mealli, *J. Organomet. Chem.* 417 (1991) C32–C35.
- [48] S. Kozuch, S. Shaik, *Acc. Chem. Res.* 44 (2011) 101–110.
- [49] J.M. Gonzales, R.S. Cox III, S.T. Brown, W.D. Allen, H.F. Schaefer III, *J. Phys. Chem. A* 105 (2001) 11327–11346.